Demo Retrofit Study of a Chinese Inspired Cell Technology

Marc Dupuis and Valdis Bojarevics

Abstract

For many years, the authors have been demonstrating their cell modeling tools and cell retrofit skills using those modeling tools to present demonstration cell retrofit studies. One recent series of cell retrofit studies leads to the presentation of a cell design predicted to be able to operate at 10 kWh/kg of Al. The authors now embark on a new demonstration retrofit study this time using a Chinese cell technology inspired base case as a starting point. There are plenty of public domain information on Chinese cell technology: potshell, busbar and lining design, so that Chinese cell technology inspired base case cell design is quite similar to existing Chinese cell technologies. This first retrofit study aims at demonstrating the huge potential of productivity increase that those existing Chinese cell technologies represent without compromising the power efficiency.

Keywords

Mathematical modeling • Amperage creep • Copper insert • Cell heat balance

Introduction

To follow-up on the series of publications [1–16] on the retrofit of a VAW-inspired 300 kA base case [17] that culminated in the design of a wide cell operating at 530 kA and 10.0 kWh/kg Al, the authors decided to perform a similar retrofit exercise this time starting from a Chinese design inspired base case. There are plenty of public domain information on Chinese cell technologies. For example, there is a US patent [18] that describes a 400 kA cell design. The potshell design is presented in Figs. 1 and 2 of said patent, while the anode panel layout using 48 anode blocks is presented in Fig. 5. The 4 stubs in line per anode block design is presented in Fig. 4b of the same document, while the lining design is presented in Fig. 8. Finally, the busbar design with 6 risers is presented in Fig. 9 of said reference [18].

Figure 1, which is Fig. 6 in [19], presents three similar busbar design in 3D this time. All those busbars are of the asymmetric, internal compensation type. They use 6 single risers, which means that the sections of the downstream side busbars are much smaller that the sections of the upstream side busbars that run on a much longer path. On the potshell side, we can see the SY350/SY400 potshell model in Fig. 2, which is Fig. 5 of [20]. This is the exact same type of potshell design presented in Figs. 1 and 2 of [18]. In Fig. 2, we can see that the SY350/SY400 cell design is using 24 cathode blocks with double bars per cathode block. Finally, on the anode and cathode design, Fig. 3, which is Fig. 9 in [21], presents a very commonly used cell layout in Chinese cell designs utilizing 24 cathode blocks and 48 anodes with 4 stubs in line. We can see the NEUI500 cell lining topology in Fig. 4, which is the Fig. 5 of [22]. Other details on typical Chinese cell lining design are given in [23].

Generic Chinese-Inspired 420 kA Base Case Models

Of all the available public domain information on Chinese cell technologies, the authors concentrated on the 420 kA cell technology presented in [21] and [23] and on the busbar presented in Fig. 6a in [19] to construct a generic Chinese-inspired 420 kA case set of models that will be used as base case for the new demo retrofit study. The generic 420 kA cell design is using the exact layout presented in Fig. 3. It was first reconstructed in HHCellVolt [24]—Fig. 5 presents

M. Dupuis (✉)
GéniSim Inc, 3111 Alger St, Jonquière,
Québec G7S 2M9, Canada
e-mail: marc.dupuis@genisim.com

V. Bojarevics
School of Computing and Mathematics, University of Greenwich,
30 Park Row, London, SE10 9LS, UK
e-mail: V.Bojarevics@gre.ac.uk

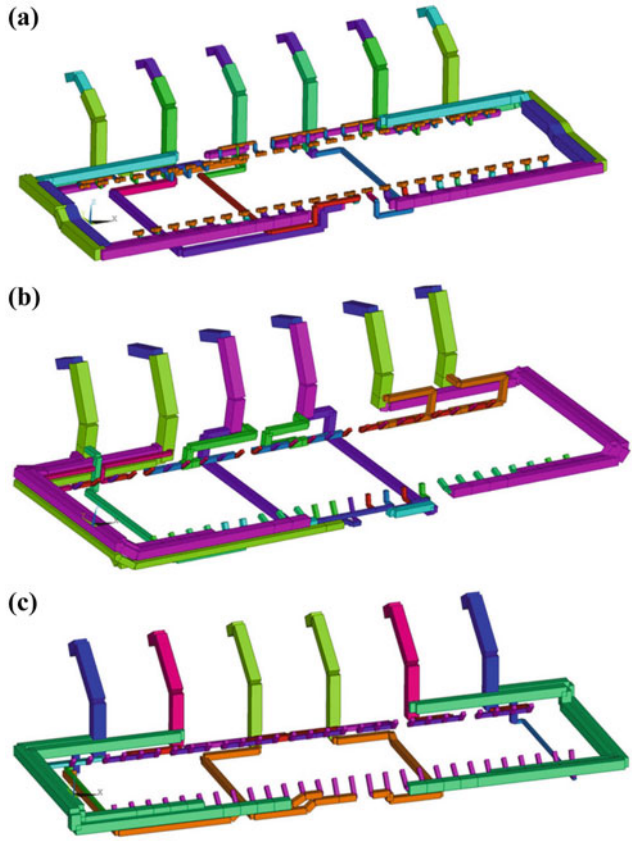

Fig. 1 Three representative busbars of 400 kA cells: **a** GY420; **b** SY400; **c** NEUI400 (Fig. 6 in [19])

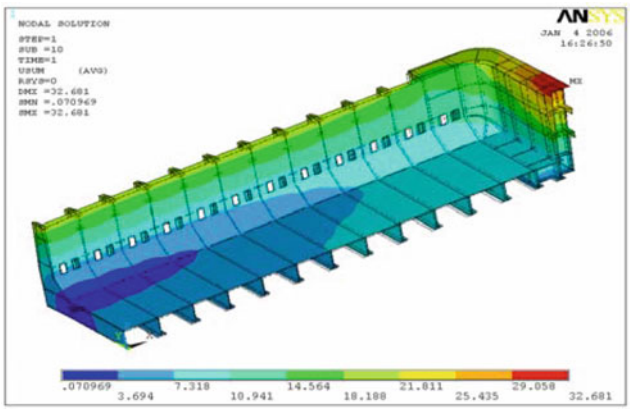

Fig. 2 Shell thermo-stress modeling, [mm], of SY350/SY400 cell potshell design (Fig. 5 in [20])

the anode panel layout produced by HHCellVolt with the selected anode size. The resulting current density is 0.77 A/cm^2 which is very typical anodic current density in China.

The generic half anode model operating at that anodic current density is presented in Fig. 6 and the predicted anode drop is 325 mV. The corresponding generic cathode side slice model is presented in Fig. 7, the predicted cathode drop

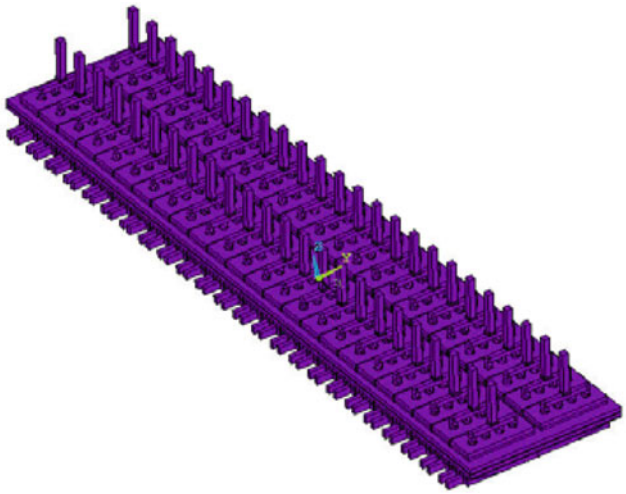

Fig. 3 Generic parametric model with 24 cathode blocks and 48 anodes having each 4 stubs in line (Fig. 9 in [21])

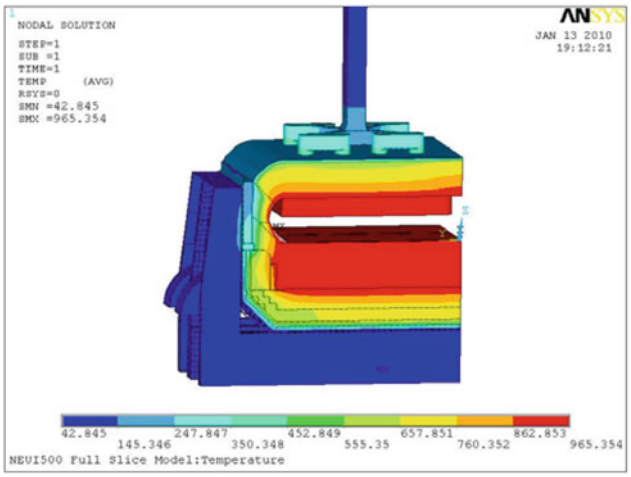

Fig. 4 Thermo-electric model, [°C], of NEUI500 cell design showing the lining design topology (Fig. 5 in [22])

is 315 mV. The MHD-Valdis cell stability model is presented next in Fig. 8. Again, the potshell geometry is inspired from Figs. 1 and 2 of [18] and the busbar from Fig. 1a. The busbar voltage drop is 200 mV.

Using the above presented ohmic resistances and 4.5 cm of anode to cathode distance (ACD), HHCellVolt can be used to calculate the cell voltage, the cell energy consumption and the cell internal heat. Results are presented in Fig. 9: the cell voltage is calculated to be 4.26 V, the cell internal is 843 kW and the cell energy consumption is 13.51 kWh/kg Al. That last result is a bit high to be typical but is the result of all our assumptions on the cell design and cell operating conditions.

On the cell stability prediction of our generic 420 kA base case cell design, the vertical component of the magnetic field (Bz) in the middle of the metal pad is presented in Fig. 10.

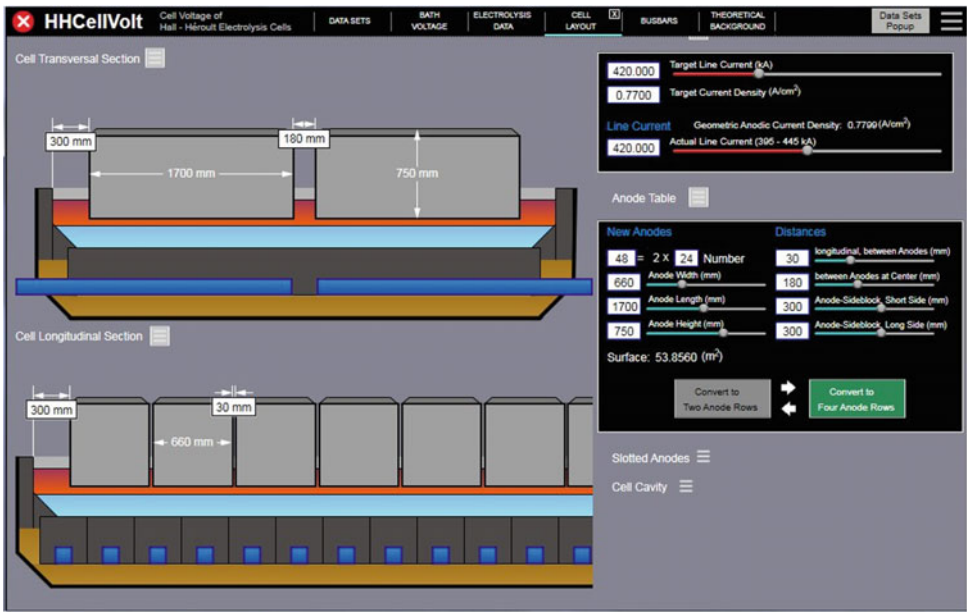

Fig. 5 Generic base case anode panel layout produced by HHCellVolt [24]

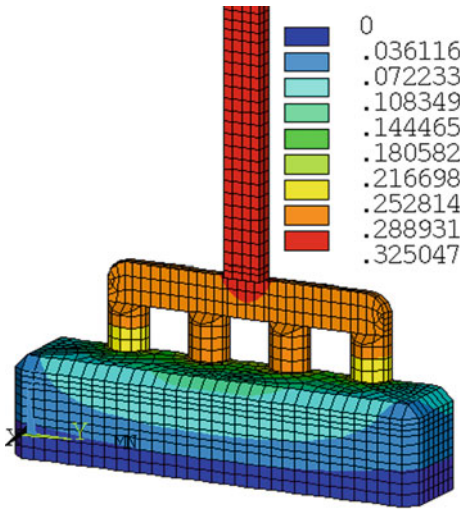

Fig. 6 Generic base case half anode T/E model voltage drop, [V], at 420 kA

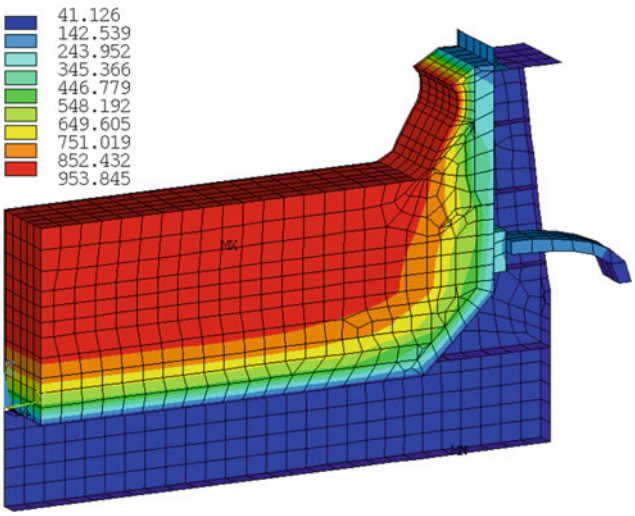

Fig. 7 Generic base case cathode side slice T/E model temperature, [°C], at 420 kA

The corresponding steady-state metal pad velocity is presented in Fig. 11 while the steady-state bath-metal interface deformation is presented in Fig. 12. Those steady-state results can be obtained relatively quickly with MHD-Valdis, yet the true measure of cell stability prediction is the dynamic response to a perturbation introduced on top of the steady-state solution. Figure 13 shows the obtained dynamic response when using a typical coefficient of friction for the cathode floor of cf = 0.06. In a real industrial application, the selection of the value of that coefficient of friction would need to be established by comparing MHD-Valdis cell stability predictions against the results obtained by an ACD squeezing test (like those presented in Figs. 16 and 17 of [25]). Using cf = 0.06, the cell is predicted to be very stable.

Dyna/Marc is the final model that need to be created to finish to characterize the operating conditions of that generic Chinese inspired 420 kA base case cell design. Dyna/Marc is a 1D+ dynamic cell simulator [26] that can be used to calculate the steady-state cell heat balance in addition to the cell voltage calculations performed by HHCellVolt. The summary of the steady-state conditions calculated by Dyna/Marc is presented in Table 1. In addition to the cell voltage, cell internal heat and cell energy consumption calculations, Dyna/Marc predicts the cell current efficiency (user input in HHCellVolt), the cell superheat (employing user defined bath to ledge and metal to ledge heat transfer coefficients) and the corresponding cell operating temperature (user input

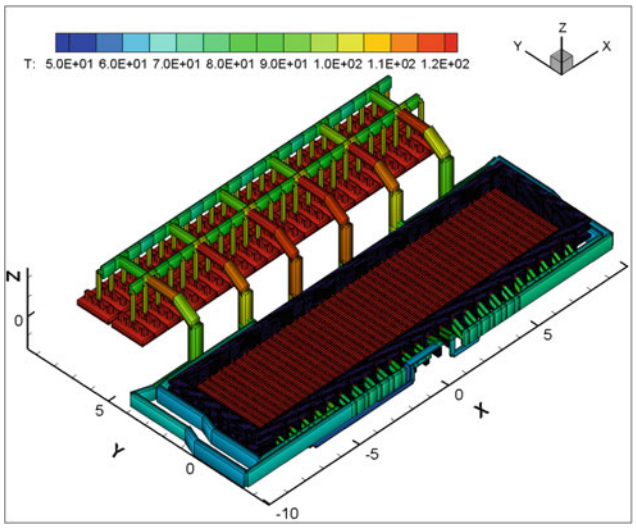

Fig. 8 Generic base case MHD-Valdis cell stability model, [°C], at 420 kA

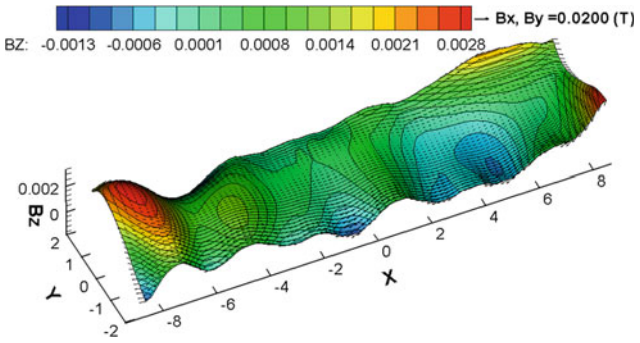

Fig. 10 Calculated BZ in the middle of the metal pad at 420 kA

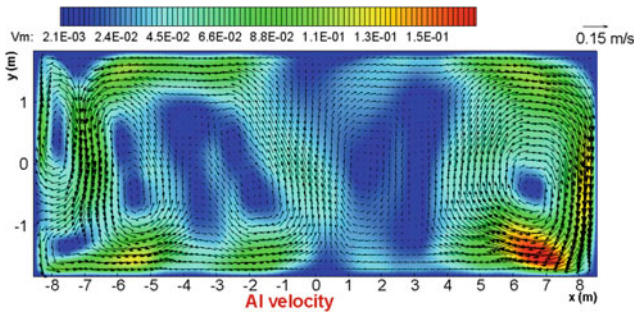

Fig. 11 Calculated vertically averaged steady-state velocity in the metal pad at 420 kA

in HHCellVolt). Dyna/Marc also calculates the average ledge thickness at the bath and metal levels. The 3D cathode side slice also calculates the average ledge thickness at the bath and metal levels and does so with more accuracy.

This summarize the presentation of the models results for the 420kA base case or starting point of this new demonstration retrofit study. When compared with key process indicators (KPI) presented by aluminum producers operating outside of China, those KPI, typical of Chinese cell operation, demonstrate the tremendous potential for production creep. This can be achieved by increasing the amperage and decreasing the ACD while maintaining the cell superheat. The aim of this demonstration retrofit study will be to do just that in several cell retrofit steps.

Fig. 9 Generic base case cell voltage and cell internal heat calculated by HHCellVolt [24] at 420 kA

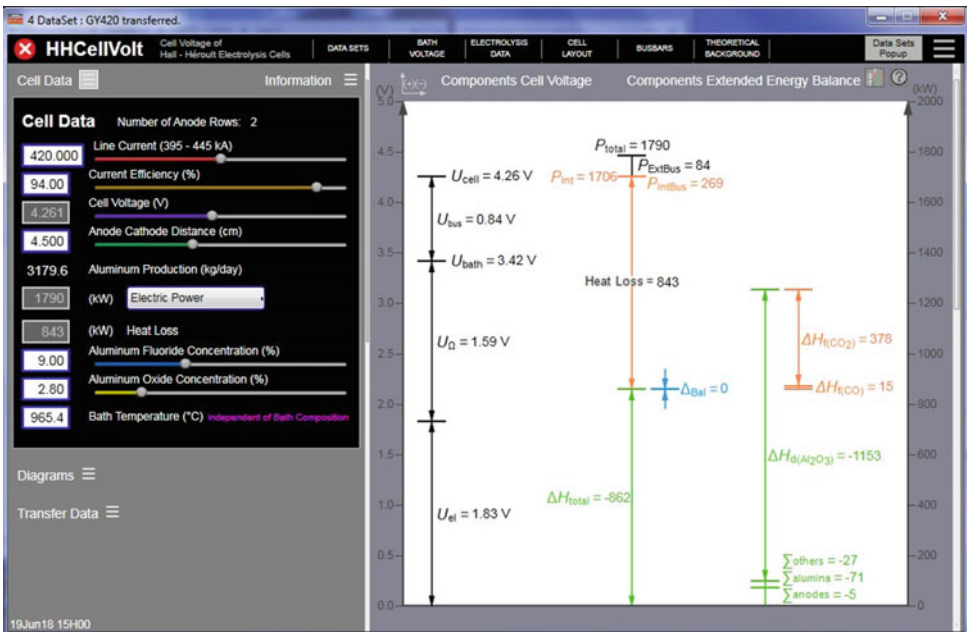

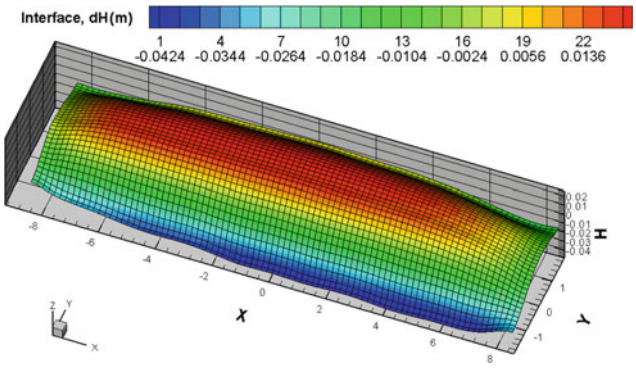

Fig. 12 Calculated steady-state deformation of the bath-metal interface at 420 kA

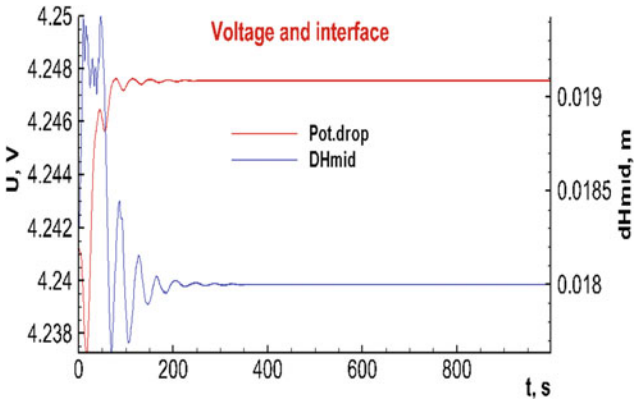

Fig. 13 Calculated dynamic response to an interface perturbation of the generic 420 kA base case cell design

Table 1 Dyna/Marc 420 kA cell results summary

Steady state solution		
Cell amperage	420.0	[kA]
Anode to cathode distance	4.50000	[cm]
Operating temperature	965.483	[C]
Ledge thickness, bath level	13.73070	[cm]
Ledge thickness, metal level	6.61534	[cm]
Bath chemistry		
Bath ratio	1.21630	[kg/kg]
Cone, of excess aluminum fluoride	9.00000	[%]
Cone, of dissolved alumina	2.80000	[%]
Cone, of calcium fluoride	5.00000	[%]
Cone, of lithium fluoride	1.00000	[%]
Heat balance		
Superheat	5.1007	[C]
Cell energy consumption	13.4852	[kWh/kg]
Internal heat generation	843.156	[kW]
Electrical characteristics		
Current efficiency	93.6961	[%]
Anode current density	0.779857	[A/cm*cm]
Bath resistivity	0.433139	[ohm-cm]
Cell pseudo-resistance	6.16450	[micro-ohm]
Bath voltage	1.50769	[V]
Electrolysis voltage	1.87410	[V]
Cell voltage	4.23909	[V]
Voltage to make the metal	2.02427	[V]

First Retrofit Step: 450 kA Cell Design

This first cell retrofit design step is very conservative, the anode length being increased by 5 cm (to 1.75 m) thus reducing the anode to side wall distance (ASD) by 5 cm to 25 cm. This is the only cell design change and there are only two cell operating condition changes: the cell amperage is increased by 30 kA (to 450 kA) and the ACD is reduced to 3.9 cm. The modified half anode model is rerun first to assess the change of anode voltage drop and anode panel heat loss. The new anode isotherms are presented in Fig. 14. The predicted new anode voltage drop is 347 mV.

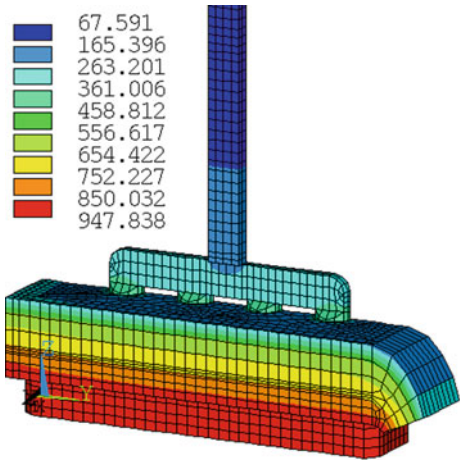

Fig. 14 Half anode model isotherms at 450 kA, [°C]

The cathode slice model and Dyna/Marc models are rerun next. The Dyna/Marc results summary is presented in Table 2.

By comparing Tables 1 and 2, we can see that the anodic current density increases to 0.81 A/cm^2 despite the increase of the anode length. The anode panel heat dissipation has also increased and ACD was decreased, the net results being that the cell superheat was not much affected. The next and final step is to assess the change in cell stability due to both the increase of the cell amperage and the reduction of the cell ACD. Figure 15 presents the dynamic response to a cell perturbation for the 450kA cell. Again, the cell is predicted to be quite stable. At this stage in a real cell retrofit scenario, that new design would be tested in a booster section and then implemented to the full smelter.

Second Retrofit Step: 480 kA Cell Design

That second cell retrofit effort involves more significant changes as it concerns the cathode design this time. The first change is to replace the semi-graphic cathode block type by a 100% graphic cathode block type. In the cathode model, HC3 type was replaced by HC10 (see [27] for technical specifications). A 4 cm × 4 cm section copper insert was added to the collector bar for most of the inside collector bar length up to the pier region, in order not to increase too

Table 2 Dyna/Marc 450 kA cell results summary

Steady state solution		
Cell amperage	450.0	[kA]
Anode to cathode distance	3.90000	[cm]
Operating temperature	966.150	[C]
Ledge thickness, bath level	11.74140	[cm]
Ledge thickness, metal level	5.28914	[cm]
Bath chemistry		
Bath ratio	1.21630	[kg/kg]
Cone, of excess aluminum fluoride	9.00000	[%]
Cone, of dissolved alumina	2.80000	[%]
Cone, of calcium fluoride	5.00000	[%]
Cone, of lithium fluoride	1.00000	[%]
Heat balance		
Superheat	5.7681	[%]
Cell energy consumption	13.3713	[kWhr/kg]
Internal heat generation	882.342	[kW]
Electrical characteristics		
Current efficiency	93.8120	[%]
Anode current density	0.811688	[A/cm*cm]
Bath resistivity	0.432809	[ohm-cm]
Cell pseudo-resistance	5.68550	[micro-ohm]
Bath voltage	1.40702	[V]
Electrolysis voltage	1.88382	[V]
Cell voltage	4.20847	[V]
Voltage to make the metal	2.02636	[V]

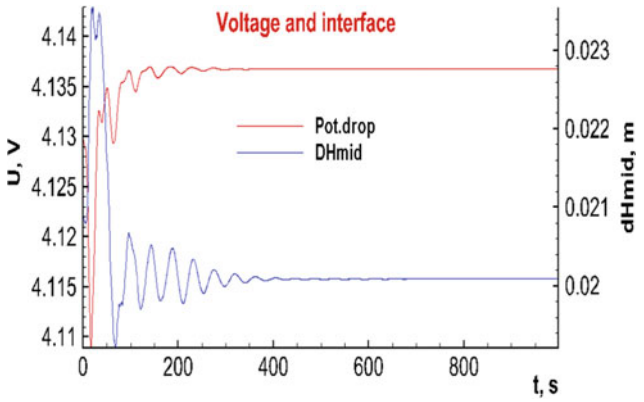

Fig. 15 Calculated dynamic response to an interface perturbation of the retrofitted 450 kA case cell design

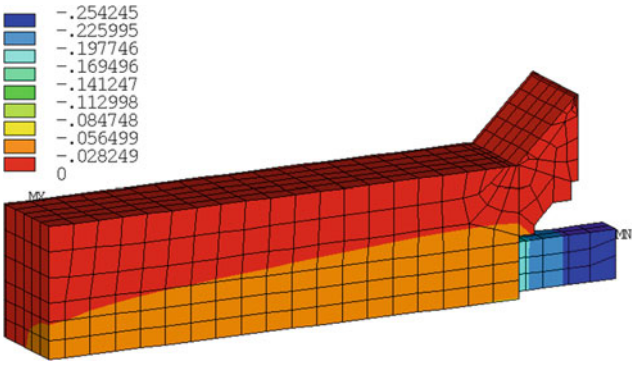

Fig. 16 480 kA cathode side slice T/E model voltage drop, [V]

much the collector bar heat losses. Finally, the dry barrier lining material so popular in China was replaced by the new Skamolbar-LE sodium resistant semi-insulating material [28] already used once in [16]. On the cell operation side, the cell ACD was further reduced to 3.5 cm and the cell amperage was further increased to 480 kA. As we can see in Fig. 16, the cathode side slice T/E model predicts a significant reduction of the cathode voltage drop (down to 254 mV) despite the increase of amperage. The half anode model is also rerun to be able to feed the new anode voltage drop and anode panel heat losses to Dyna/Marc. Those new Dyna/Marc summary results for the 480 kA retrofit cell design are presented in Table 3. As Table 3 indicates, this time the cell internal heat increased and so did the cell superheat, but not that significantly. The anode current density continues to increase, this time reaching 0.87 A/cm^2, and getting to the range where having very good quality anodes is a requirement.

On the cell stability side, adding the copper insert helps to reduce the horizontal currents hence improving the cell

Table 3 Dyna/Marc 480 kA cell results summary

Steady state solution		
Cell amperage	480.0	[kA]
Anode to cathode distance	3.50000	[cm]
Operating temperature	967.348	[C]
Ledge thickness, bath level	9.12748	[cm]
Ledge thickness, metal level	3.54653	[cm]
Bath chemistry		
Bath ratio	1.21630	[kg/kg]
Cone, of excess aluminum fluoride	9.00000	[%]
Cone, of dissolved alumina	2.80000	[%]
Cone, of calcium fluoride	5.00000	[%]
Cone, of lithium fluoride	1.00000	[%]
Heat balance		
Superheat	6.9658	[C]
Cell energy consumption	13.0925	[kWhr/kg]
Internal heat generation	900.402	[kW]
Electrical characteristics		
Current efficiency	94.4794	[%]
Anode current density	0.865801	[A/cm*cm]
Bath voltage	1.38184	[V]
Electrolysis voltage	1.89972	[V]
Cell voltage	4.15004	[V]
Voltage to make the metal	2.03776	[V]

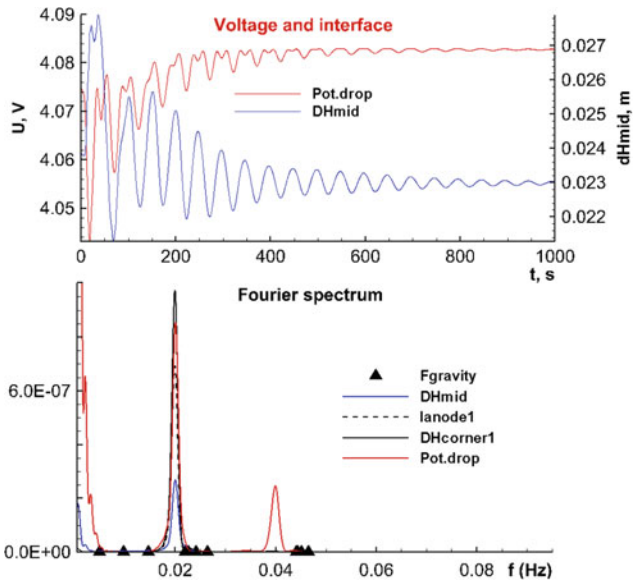

Fig. 17 Calculated dynamic response to an interface perturbation of the retrofitted 480 kA case cell design

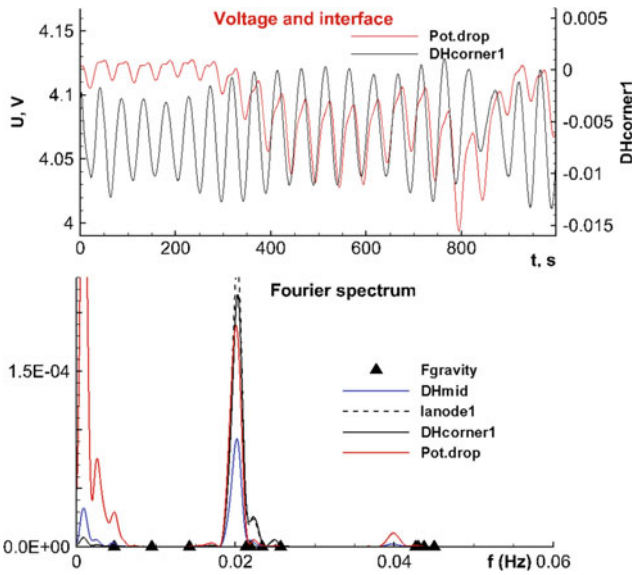

Fig. 18 Calculated dynamic response to an interface perturbation of the retrofitted 500 kA case cell design (20 cm)

stability. This is counteracting to a certain point the negative impacts of both continuing to increase the cell amperage and reducing the cell ACD.

Figure 17 presents the dynamic response to an interface perturbation for the 480 kA cell. The perturbation is damping less rapidly generating a sharp 0.02 Hz frequency or 50 s period rotating wave. It is clear that as we progress towards increasing the anode current density and reducing the cell ACD, the cell stability is decreasing, putting pressure on the cell control system to avoid cell instability-promoting events (like sludge formation) with increasing alumina feeding rate. This is the reason why, in a real cell retrofit scenario, the new considered cell design needs to be tested in a booster section and the cell control logic improved before it could be successfully implemented to the full smelter.

Third Retrofit Step: 500 kA Cell Design

The third cell retrofit design step involves less cell design changes. It is safer at this point to use smaller steps to test how far we can push the amperage increase and the ACD reduction before the cell become unstable. To be on the safe side, the copper insert section has been increased to 8 cm × 4 cm. This is the only cell design change. On the cell operation side, the cell amperage has been increased to 500 kA while the ACD has been reduced to 3.25 cm.

After running the half anode T/E model and the cathode slice T/E model, the Dyna/Marc model is updated with the new anode and cathode voltage drops and the new anode panel heat loss and rerun. The cell internal heat continues to increase but the impact on the cell superheat is still quite acceptable. Those results are not reported in the paper. The cell stability was next tested in MHD-Valdis with the results presented in Fig. 18. Clearly, the critical cell stability prediction has been reached. The initial perturbation is not yet growing but is not damping anymore, generating everlasting voltage noise (again at 0.02 Hz).

This was considered unacceptable, so it was decided to improve the cell stability by increasing the metal level by 5 cm (to 25 cm). Increasing the metal pad thickness is known to improve the cell stability because it decreases the steady-state horizontal current intensity and it would also decrease the intensity of the horizontal current generated by a wave propagation. Yet it has an extra stabilizing effect not often discussed: it reduces the average Bz intensity in the metal pad. Figure 19 presents the Bz for the 500 kA cell case with 20 cm metal pad thickness, while Fig. 20 is presenting the Bz for the 500 kA cell case with 25 cm metal pad thickness. This is a quite significant Bz intensity reduction.

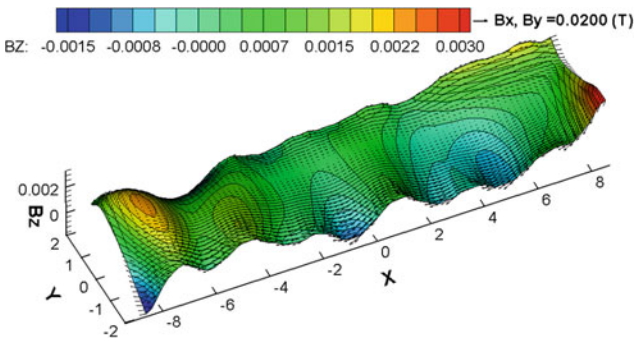

Fig. 19 Calculated BZ in the middle of the metal pad (20 cm) at 500 KA

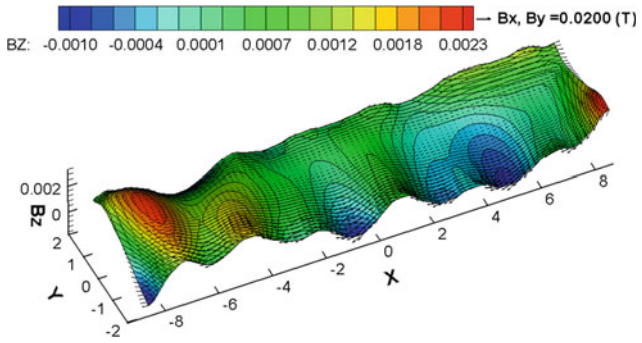

Fig. 20 Calculated BZ in the middle of the metal pad (25 cm) at 500 kA

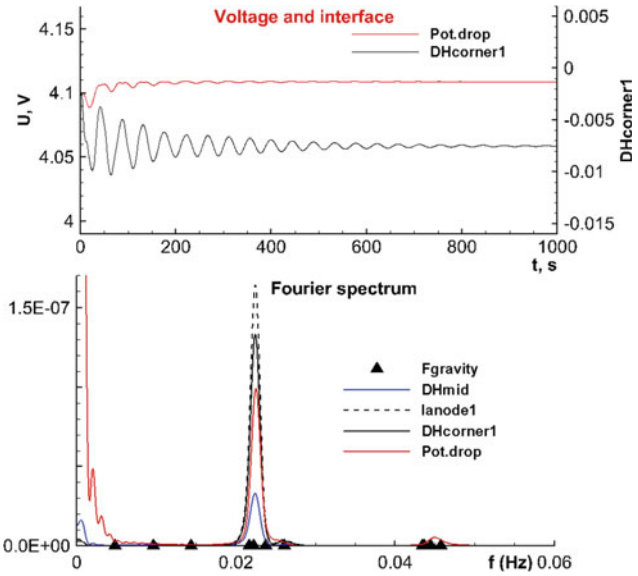

Fig. 21 Calculated dynamic response to an interface perturbation of the retrofitted 500 kA case cell design (25 cm)

Figure 21 presents the results of the repeated cell stability analysis, this time using 25 cm of metal pad thickness. The cell stability has been remarkably improved.

Following this change of operating conditions, the cathode side slice T/E model had to be rerun and finally the global cell heat balance conditions reassessed by rerunning Dyna/Marc.

Table 4 presents the Dyna/Marc results summary for the 500kA cell case using 25 cm of metal pad thickness. This increase of metal pad thickness also helped reducing the cell superheat which brings it back almost to the initial cell superheat at 420 kA. The anode current density reached 0.90 A/cm^2 which is still below the anode current density of the

Table 4 Dyna/Marc 500 kA cell results summary

Steady state solution		
Cell amperage	500.0	[kA]
Anode to cathode distance	3.25000	[cm]
Operating temperature	965.588	[C]
Ledge thickness, bath level	13.38490	[cm]
Ledge thickness, metal level	6.38481	[cm]
Bath chemistry		
Bath ratio	1.21630	[kg/kg]
Cone. of excess aluminum fluoride	9.00000	[%]
Cone. of dissolved alumina	2.80000	[%]
Cone. of calcium fluoride	5.00000	[%]
Cone. of lithium fluoride	1.00000	[%]
Heat balance		
Superheat	5.2054	[C]
Cell energy consumption	13.1008	[kWhr/kg]
Internal heat generation	938.821	[kW]
Electrical characteristics		
Current efficiency	94.8324	[%]
Ancde current density	0.901876	[A/cm*cm]
Bath voltage	1.37046	[V]
Electrolysis voltage	1.91074	[V]
Cell voltage	4.16817	[V]
Voltage to make the metal	2.04322	[V]

highly productive cell technologies operating outside of China. The current efficiency (CE) prediction has increased to 94.8% despite the ACD reduction because the Solli's model [29] that is used to compute CE is sensitive to the anode current density and is not sensitive to the cell ACD. This is consistent with KPI reported around the world.

Fourth and Final Retrofit Step: 520 kA Cell Design

Improving the cell stability by increasing the metal pad thickness opened the door to this fourth and final retrofit step reducing the cell ACD to 3.0 cm and pushing the cell amperage up to 520 kA, which is 100 kA more that the initial base case value. To be able to achieve that level of amperage without increasing too much the anodic current density, the anode length was increased to 1.78 m further reducing the ASD to 22 cm. The half anode and cathode side slice cathode models were run one last time. The final results for these two models are presented in Tables 5 and 6.

The convergence of the ledge profile is part of the solution of the cathode side slice model. A quite acceptable final ledge profile is presented in Fig. 22.

Dyna/Marc independently computes similar ledge thickness using a 1D thermal model that is far less sophisticated that the 3D cathode side slice model, so when available, it is always better to rely on the 3D results. Dyna/Marc is used to integrate the separate anode and cathode T/E models. The final Dyna/Marc 520 kA summary results are presented in Table 7. Again, the final cell superheat at 520 kA is remarkably similar to the initial one at 420 kA which was the main strategy of the cell retrofit study. The four steps of the cell retrofit study are summarized in Table 8. It is noticeable that a (520 × 94.6)/(420 × 93.7) = 25% increase of the cell productivity was obtained without compromising the cell energy consumption: on the contrary, it was reduced by 0.63 kWh/kg Al, from 13.49 to 12.86 kWh/kg Al (or by 4.7%). Nevertheless, the smelter would require about (520 × 4.08)/(420 × 4.24) = 19% more power from the grid.

An extra 100 kA has now been added into a busbar network designed to be balanced while operating at 420 kA.

Table 5 Anode heat balance

Heat balance table Half anode model: 520 kA			
Anode panel heat lost	kW	W/m^2	%
Crust to air	240.74	3338.54	53.47
Studs to air	166.53	5282.00	36.99
Aluminum rod to air	42.97	616.34	9.54
Total Anode Panel Heat Lost	450.24		100.00

Table 6 Cathode heat balance

Heat balance table Side slice model: 520 kA			
Cathode heat lost	kW	W/m^2	%
Shell wall above bath level	75.49	1907.73	15.79
Shell wall opposite to bath	52.66	4606.01	11.02
Shell wall opposite to metal	54.22	7113.68	11.34
Shell wall opposite to block	73.86	4049.26	15.45
Shell wall below block	21.57	935.01	4.51
Shell floor	23.03	374.53	4.82
Cradle opposite to bath	14.79	1044.76	3.10
Cradle opposite to metal	14.80	933.09	3.10
Cradle opposite to block	22.73	527.13	4.76
Cradle opposite to brick	7.66	181.55	1.60
Cradle below floor level	13.54	74.24	2.83
Bar and flex to air	79.48	2519.88	16.63
End of flex to busbar	24.15	27957.02	5.05
Total cathode heat lost	477.97		100.00

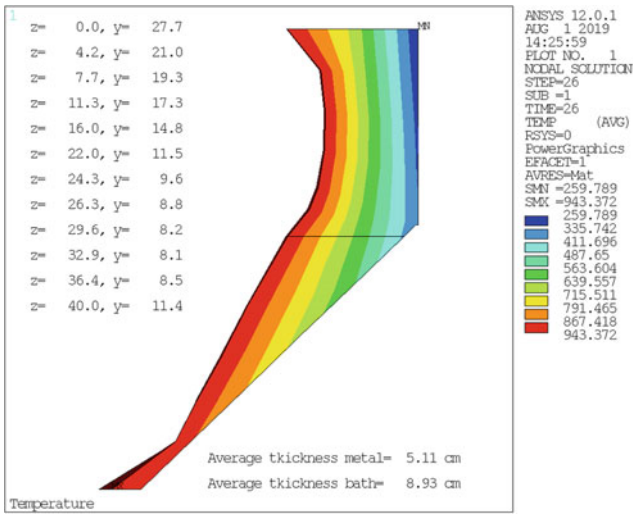

Fig. 22 Converged ledge profile of the 520 kA cell case, [°C]

Is that balance between the upstream and the downstream side maintained at 520 kA? The answer to that question is part of the MHD-Valdis cell stability analysis. The cathodic upstream/downstream current partition is calculated to be 49.84% upstream and 50.16% downstream for the 420 kA base case cell. For the 520 kA cell case, without any change to the busbar design itself, the current partition changed to 50.41% upstream and 49.59% downstream. Clearly, the downstream busbars are heating up faster and hence are getting more resistive than the bigger section upstream busbars. Yet the results indicate that this is not significant enough to justify any changes to the busbar network design.

The increase of busbar temperature alone can be a source of concern. Figure 23 presents the busbar temperature results for the initial 420 kA base case while Fig. 24, those for the 520 kA cell case. The maximum temperature in the small section downstream busbar increased about 50 °C going from about 140 °C to about 190 °C. This will generate extra thermal expansion that may overstress some welds but this problem can be addressed [30].

Figure 25 presents the corresponding obtained depth averages Bz still at 25 cm of metal pad thickness, not so different from the one presented in Fig. 20.

The corresponding depth averages steady-state metal flow is presented in Fig. 26 while the steady-state bath-metal interface deformation is presented in Fig. 27. The metal flow is gaining momentum with the maximum speed increasing from 15 cm/s to 18 cm/s (or by 20%). More significantly, the amplitude of the bath-metal deformation increased from 5.6 cm to 8.71 cm (or by 56%). Apart from completely

Table 7 Dyna/Marc 520 kA cell results summary

Steady state solution		
Cell amperage	520.0	[kA]
Anode to cathode distance	3.00000	[cm]
Operating temperature	966.140	[C]
Ledge thickness, bath level	11.76975	[cm]
Ledge thickness, metal level	5.30804	[cm]
Bath chemistry		
Bath ratio	1.21630	[kg/kg]
Cone, of excess aluminum fluoride	9.00000	[%]
Cone, of dissolved alumina	2.80000	[%]
Cone, of calcium fluoride	5.00000	[%]
Cone, of lithium fluoride	1.00000	[%]
Heat balance		
Superheat	5.7574	[C]
Cell energy consumption	12.8580	[kwhr/kg]
Internal heat generation	928.885	[kW]
Electrical characteristics		
Current efficiency	94.6091	[%]
Anode current density	0.922143	[A/cm*cm]
Bath voltage	1.24789	[V]
Electrolysis voltage	1.91219	[V]
Cell voltage	4.08130	[V]
Voltage to make the metal	2.03963	[V]

Table 8 Summary of the demonstration retrofit study ANSYS (A), Dyna/Marc (D/M), Total (T), Busbar (B)

Amperage	420 kA	450 kA	480 kA	500 kA	520 kA
Nb. of anodes	48	48	48	48	48
Anode size	1.70 m × 0.66 m	1.75 m × 0.66 m	1.75 m × 0.66 m	1.75 m × 0.66 m	1.78 m × 0.66 m
Nb. of anode studs	4 per anode	4 per anode	4 per anode	4 per anode	4 per anode
Anode stud diameter	16.5 cm	16.5 cm	16.5 cm	16.5 cm	16.5 cm
Anode cover thickness	14 cm	14 cm	14 cm	14 cm	14 cm
Nb. of cathode blocks	24	24	24	24	24
Cathode block length	3.68 m	3.68 m	3.68 m	3.68 m	3.68 m
Type of cathode block	HC3	HC3	HC10	HC10	HC10
Collector bar size	18 cm × 10 cm	18 cm × 10 cm	18 cm × 10 cm	18 cm × 10 cm	18 cm × 10 cm
Copper insert size	0 cm × 0 cm	0 cm × 0 cm	4 cm × 4 cm	8 cm × 4 cm	8 cm × 4 cm
Type of side block	SiC	SiC	SiC	SiC	SiC
Side block thickness	9 cm	9 cm	9 cm	9 cm	9 cm
ASD	30 cm	25 cm	25 cm	25 cm	22 cm
Calcium silicate thickness	8.0 cm	8.0 cm	8.0 cm	8.0 cm	8.0 cm
Material below blocks	Dry Barrier	Dry Barrier	Skamolbar-LE	Skamolbar-LE	Skamolbar-LE
Inside potshell size	17.34 × 4.32 m	17.34 × 4.32 m	17.34 × 4.32 m	17.34 × 4.32 m	17.34 × 4.32 m
ACD	4.5 cm	3.9 cm	3.5 cm	3.25 cm	3.0 cm
Anode current density	0.77 A/cm^2	0.81 A/cm^2	0.87 A/cm^2	0.90 A/cm^2	0.92 A/cm^2
Metal level	20 cm	20 cm	20 cm	25 cm	25 cm
Excess AlF_3	9.00%	9.00%	9.00%	9.00%	9.00%
Anode drop (A)	325 mV (T)	347 mV (T)	371 mV (T)	386 mV (T)	400 mV (T)
Cathode drop (A)	315 mV (T)	337 mV (T)	253 mV (T)	245 mV (T)	256 mV (T)
Busbar/External drop (A)	200 mV (B)	214 mV (B)	229 mV (B)	240 mV (B)	248 mV (B)
Anode panel heat loss (A)	382 kW (T)	422 kW (T)	435 kW (T)	442 kW (T)	450 kW (T)
Cathode total heat loss (A)	461 kW (T)	460 kW (T)	465 kW (T)	497 kW (T)	478 kW (T)
Operating temperature (D/M)	965.5 °C	966.2 °C	967.3 °C	965.6 °C	966.1 °C
Liquidus superheat (D/M)	5.1 °C	5.8 °C	7.0 °C	5.2 °C	5.8 °C
Bath ledge thickness (A)	9.53 cm	9.51 cm	9.44 cm	9.43 cm	8.93 cm
Metal ledge thickness (A)	6.03 cm	5.91 cm	5.66 cm	5.62 cm	5.11 cm
Current efficiency (D/M)	93.7%	93.8%	94.5%	94.8%	94.6%
Internal heat (D/M)	843 kW	882 kW	900 kW	939 kW	929 kW
Cell Voltage (D/M)	4.24 V	4.21 V	4.15 V	4.17 V	4.08 V
Energy consumption (D/M)	13.49 kWh/kg	13.37 kWh/kg	13.09 kWh/kg	13.10 kWh/kg	12.86 kWh/kg

changing the busbar design to use a different type of magnetic compensation, there is not much that can be done about the amplitude of the bath-metal deformation, but this increase is not considered to be a problem.

Finally, Fig. 28 presents the most important results of the MHD-Valdis cell stability analysis, namely, the dynamic response to a perturbation to the steady-state bath-metal interface deformation. It is less stable than the previous case, but still quite stable as the interface perturbation is damping rapidly.

This concludes the presentation of the results of this last retrofit step from 500 to 520 kA. It is the authors' belief that they are good enough to justify a potential investment regarding the construction of prototypes to test the viability of this cell design and those cell operating conditions. The prototyping period will permit to make adjustments to the cell control logic allowing to operate the cell in those much more challenging operating conditions in the booster section and, eventually, proceed to the implementation of that last step in the full smelter.

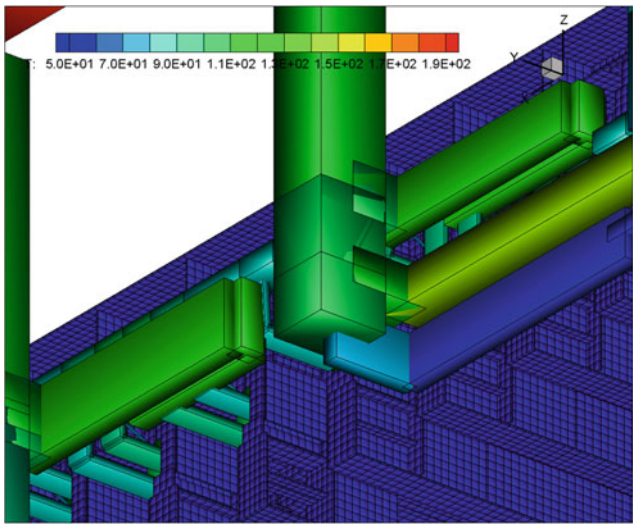

Fig. 23 Busbar temperature for the 420 kA base case cell, [°C]

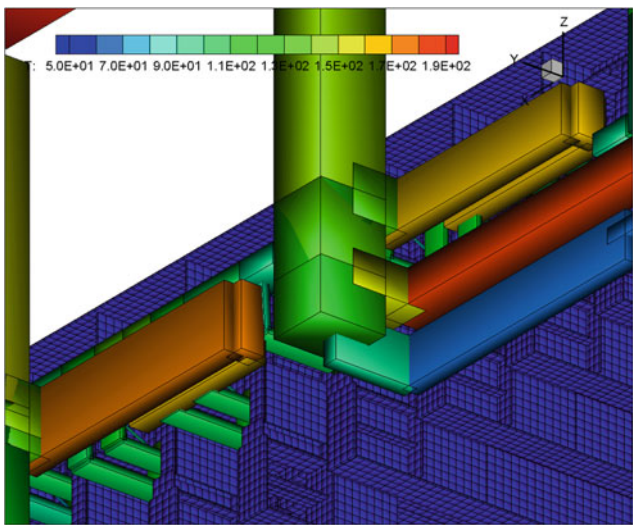

Fig. 24 Busbar temperature for the 520 kA case cell, [°C]

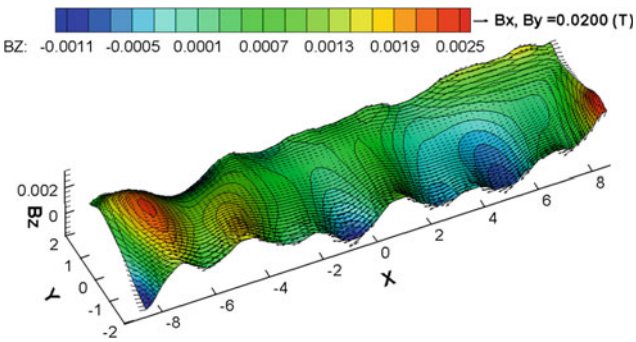

Fig. 25 Calculated BZ in the middle of the metal pad (25 cm) at 520 kA

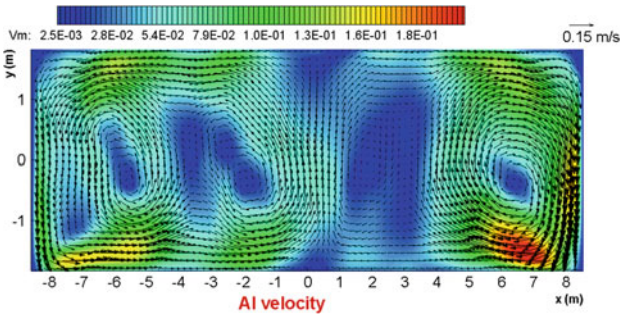

Fig. 26 Calculated vertically averaged steady-state velocity in the metal pad (25 cm) at 520 kA

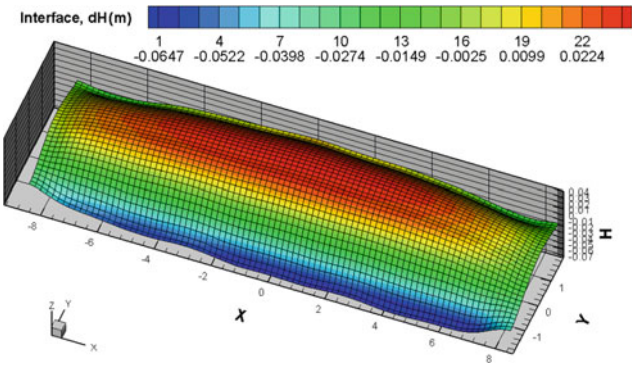

Fig. 27 Calculated steady-state deformation of the bath-metal interface (25 cm) at 520 kA

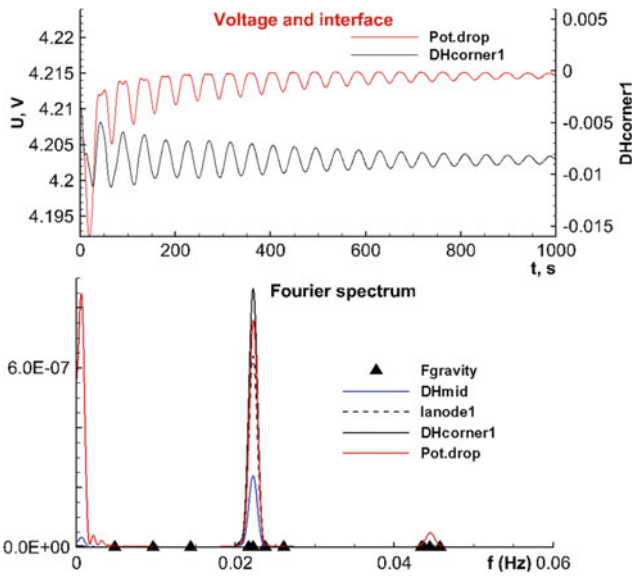

Fig. 28 Calculated dynamic response to an interface perturbation of the retrofitted 520 kA case cell design (25 cm)

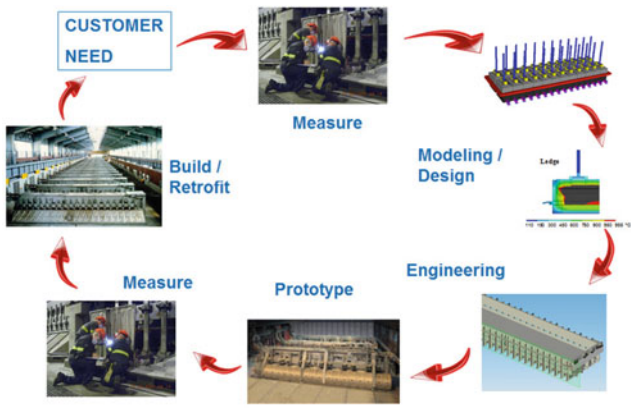

Fig. 29 Cell Development Cycle, Fig. 2 of [31]

Future Work

The obvious next step would be to repeat this retrofit exercise using a real Chinese cell technology, like the GY420 the SY400 or the NEUI400. Then, install a booster section in a smelter using that cell technology and start implementing the results of the retrofit study using the cell development cycle presented in Fig. 29, which is Fig. 2 of [31]. Each cycle involves a prototyping period in a smelter booster section or an independent cell development center and a full-scale implementation period. For that reason, each turn around requires several years of elapse time, involving two phases of cell measurements and model validation and two phases of engineering, procurement and construction. The improvement of the cell control logic during the prototyping period is also critical to the cell technology development.

Conclusions

A demonstration retrofit study of a Chinese inspired 420 kA cell design was performed to boost the amperage by 100 kA without compromising the cell heat balance or the cell stability. This was achieved while improving the cell energy consumption by reducing the cell ACD by more than the minimum required amount to compensate for the increase of anodic current density. Note that a 3 cm ACD cannot anymore be considered as being "too low" given that many successful cell technologies are now operating below this mark.

This demonstrates the enormous production creep potential of the installed Chinese aluminum industry. Yet, the development of the production creep potential in China will require the introduction of the practice of gradual cell retrofit using the cell development cycle as it is done everywhere else outside of China.

References

1. M. Dupuis, "Thermo-Electric Design of a 400 kA Cell using Mathematical Models: A Tutorial", *TMS Light Metals*, 2000, 297–302.
2. M. Dupuis, "Thermo-Electric Design of a 500 kA Cell", *ALUMINIUM 79(7/8)*, 2003, 629–631.
3. M. Dupuis, V. Bojarevics and J. Freibergs, "Demonstration Thermo-Electric and MHD Mathematical Models of a 500 kA Al Electrolysis cell", *Proceedings of the 42nd Conference on Light Metals, CIM*, 2003, 3–20.
4. M. Dupuis, V. Bojarevics and J. Freibergs, "Demonstration Thermo-Electric and MHD Mathematical Models of a 500 kA Al Electrolysis cell: Part 2", *TMS Light Metals*, 2004, 453–459.
5. M. Dupuis, "Thermo-Electric Design of a 740 kA Cell, Is There a Size Limit", *ALUMINIUM 81(4)*, 2005, 324–327.
6. M. Dupuis, V. Bojarevics and D. Richard, "MHD and pot mechanical design of a 740 kA cell" *ALUMINIUM 82(5)*, 2006, 442–446.
7. M. Dupuis and V. Bojarevics, "Retrofit of a 500 kA Cell Design into a 600 kA Cell Design", *ALUMINIUM 87(1/2)*, 2011, 52–55.
8. M. Dupuis, "A new aluminium electrolysis cell busbar network concept", *Proceedings of 33rd International ICSOBA Conference*, Dubai, UAE, 29 November—1 December 2015, Paper AL21, Travaux No. 44, 699–708.
9. M. Dupuis, "New Busbar Network Concepts Taking Advantage of Copper Collector Bars to Reduce Busbar Weight and Increase Cell Power Efficiency", *Proceedings of 34th International ICSOBA Conference*, Travaux No. 45, Quebec, Canada, 3—6 October 2016, Paper AL39.
10. M. Dupuis, "Low Energy Consumption Cell Designs Involving Copper Inserts and an Innovative Busbar Network Layout", *TMS Light Metals*, 2017, 693–703.
11. M. Dupuis and B. Welch, "Designing cells for the future—Wider and/or even higher amperage?", *ALUMINIUM 93(1/2)*, 2017, 45–49.
12. M. Dupuis, "Very Low Energy Consumption Cell Design: The Cell Heat Balance Challenge", *TMS Light Metals*, 2018, 689–697.
13. M. Dupuis, "Breaking the 11 kWh/kg Al barrier", *ALUMINIUM 94(1/2)*, 2018, 30–34.
14. M. Dupuis, "How to Limit the Heat Loss of Anode Studs and Cathode Collector Bars in Order to Reduce Cell Energy Consumption", *TMS Light Metals*, 2019, 521–531.
15. M. Dupuis, "First Attempt to Break the 10 kWh/kg barrier using an wide cell design", *ALUMINIUM 95(1/2)*, 2019, 24–29.
16. M. Dupuis, "Second attempt to break the 10 kWh/kg aluminium barrier using a wide cell design", *Proceedings of 37th International ICSOBA Conference*, Travaux No. 48, Krasnoyarsk, Russia, 16—20 September 2019.
17. V.A. Kryukovski, G.A. Sirasutdinov, J. Klein, G. Peychal-Heiling, "International cooperation and high-performance reduction in Siberia". *JOM 46(2)*, 1994, 23–25.
18. D. Lu and al., "400 kA high energy efficiency reduction pot", *US patent no 2011/0067000 A1*, 2011.
19. H. Zhang and al., "Evolution of the Busbar Structure in Large-Scale Aluminum Reduction Cells". *JOM 69(2)*, 2017, 307–314.
20. J. Zhu and al., "The advancement of new generation SY350 pot", *TMS Light Metals*, 2009, 377–379.
21. F. Yan, M. Dupuis, J. Zhou and S. Ruan, "In depth analysis of energy-saving and current efficiency improvement of aluminum reduction cells", *TMS Light Metals*, 2013, 537–542.
22. D. Lu and al., "Development of NEUI500kA Family High Energy Efficiency Aluminum Reduction Pot ('HEEP') Technology", *TMS Light Metals*, 2011, 455–460.

23. J. Zhou and M. Dupuis, “In-Depth Analysis of Lining Designs for Several 420 kA Electrolytic Cells”, *TMS Light Metals*, 2015, 685–690.
24. P. Entner, HHCellVolt AlWeb application: http://peter-entner.com/ug/windows/hhcellvolt/toc.aspx.
25. R. von Kaenel and al., “The Use of Copper in Cathodes of Aluminium Reduction Cells”, *Proceedings of 35th International ICSOBA Conference*, Travaux No. 46, Hamburg, Germany, 2—5 October 2017, Paper AL11.
26. M. Dupuis and H. Côté, “Dyna/Marc 15.0 User’s Guide”, GeniSim, 2019.
27. Carbone Savoie: Semi-graphitic, graphitic and graphitized cathodic products https://www.carbone-savoie.com/cathode-aluminium-products/.
28. SkamoAlu-Barrier-LE: https://www.skamol.com/shop/product/skamoalu-barrier-le.
29. P.A. Solli, T. Haarberg, T. Eggen, E. Skybakmoen and A. Sterten, “A Laboratory Study of Current Efficiency in Cryolitic Melts”, *TMS Light Metals*, 1994, 195–203.
30. A. F. Schneider and al., “A Thermal-Mechanical Approach for the Design of Busbars Details”, *TMS Light Metals*, 2013, 829–835.
31. B. Allano, B. Molinier and G. Jaouen, “Online Support for Amperage Creeping and Technology Brick Implementation”, *Proceedings of 35th International ICSOBA Conference*, Travaux No. 46, Hamburg, Germany, 2—5 October 2017, Paper AL08.